Pyridoxamine Protects Proteins from Functional Damage by 3-Deoxyglucosone: Mechanism of Action of Pyridoxamine†

Sergei V. Chetyrkin,‡ Wenhui Zhang,§ Billy G. Hudson,‡,|| Anthony S. Serianni,§ and Paul A. Voziyan*,‡,||

Departments of Medicine and Biochemistry, Vanderbilt University Medical Center, Nashville, Tennessee 37232, and Department of Chemistry and Biochemistry, University of Notre Dame, Notre Dame, Indiana 46556

Received June 15, 2007; Revised Manuscript Received November 5, 2007

ABSTRACT: Pyridoxamine (PM) is a promising drug candidate for treatment of diabetic nephropathy. The therapeutic effect of PM has been demonstrated in multiple animal models of diabetes and in phase II clinical trials. However, the mechanism of PM therapeutic action is poorly understood. One potential mechanism is scavenging of pathogenic reactive carbonyl species (RCS) found to be elevated in diabetes. We have suggested previously that the pathogenicity of RCS methylglyoxal (MGO) may be due to modification of critical arginine residues in matrix proteins and interference with renal cell−matrix interactions. We have also shown that this MGO effect can be inhibited by PM (Pedchenko *et al*. (2005) *Diabetes 54*, 2952−2960). These findings raised the questions of whether the effect is specific to MGO, whether other structurally different physiological RCS can act via the same mechanism, and whether their action is amenable to PM protection. In the present study, we have shown that the important physiological RCS 3-deoxyglucosone (3-DG) can damage protein functionality, including the ability of collagen IV to interact with glomerular mesangial cells. We have also demonstrated that PM can protect against 3-DG-induced protein damage via a novel mechanism that includes transient adduction of 3-DG by PM followed by irreversible PM-mediated oxidative cleavage of 3-DG. Our results suggest that, in diabetic nephropathy, the therapeutic effect of PM is achieved, in part, via protection of renal cell−matrix interactions from damage by a variety of RCS. Our data emphasize the potential importance of the contribution by 3-DG, along with other more reactive RCS, to this pathogenic mechanism.

Pyridoxamine (PM)[1] is a promising drug candidate for treatment of diabetic nephropathy and is currently on the FDA "fast track" for phase III clinical trials (*1*). In preclinical studies, it has been shown to ameliorate nephropathy and retinopathy in several animal models of diabetes (*2*−*5*). In these studies, the therapeutic effects of PM have been attributed, in part, to its scavenging of different reactive carbonyl compounds, thus ameliorating diabetic "carbonyl stress" (*6*). In the rat models of diabetes, PM treatment had a significant renoprotective effect (*7*, *8*), accompanied by a substantial decrease in plasma levels of the reactive carbonyl compounds glyoxal (GO) and methylglyoxal (MGO), and in MGO lysine dimer, a specific MGO-derived protein cross-link (*7*−*9*). PM adducts and carbonyl products of fatty acid degradation were detected in the urine of PM-treated animals, indicating that the carbonyl trapping mechanism is operative in vivo (*10*).

The mechanisms of carbonyl scavenging by PM appear to depend on the nature of the carbonyl species. In the case of the two-carbon species, GO and glycolaldehyde (GLA), PM formed five-ring adduct structures (*11*), while a different imidazolium adduct was formed in the reaction between PM and the three-carbon species MGO (*9*). PM trapping of longer carbonyl products derived from the oxidation of linoleic and arachidonic acids occurred via the formation of a transient seven-membered ring followed by a ring-opening rearrangement (*10*). However, PM did not scavenge the carbonyl product of lipid peroxidation, 4-hydroxy-2-nonenal (HNE), and did not inhibit HNE-induced cytotoxic effects (*12*; J. D. West and P. A. Voziyan, unpublished data).

3-Deoxyglucosone (3-DG) is a physiologically important RCS that may be involved in the pathogenesis of diabetic complications. The serum concentration of 3-DG is significantly elevated in diabetes (*13*, *14*), and 3-DG-derived protein adducts increase significantly in renal glomeruli and retinas of STZ-diabetic rats, in renal tissues and aortas of diabetic patients, and in human plasma proteins in renal failure (*15*−*18*). 3-DG forms during the spontaneous oxidation of glucose, from Schiff base or protein−Amadori intermediates, or as a byproduct of protein deglycation in the reaction catalyzed by fructosamine-3-kinase (*19*−*21*). Although the reactivity of 3-DG toward nucleophilic groups is considerably lower compared to that of MGO or GO (*22*), it can modify

† B.G.H. and A.S.S. have received support from National Institute of Diabetes and Digestive and Kidney Disease Research Grant DK-65138. P.A.V. has received support from National Institute of Diabetes and Digestive and Kidney Disease Research Grant DK-66415.

* To whom correspondence should be addressed. Phone: (615) 322-2089. Fax: (615) 343-7156. E-mail: paul.voziyan@vanderbilt.edu.

‡ Department of Medicine, Vanderbilt University Medical Center.

§ University of Notre Dame.

|| Department of Biochemistry, Vanderbilt University Medical Center.

[1] Abbreviations: AGE, advanced glycation end product; BSA, bovine serum albumin; CML, N^{ϵ}-(carboxymethyl)lysine; 3-DG, 3-deoxyglucosone; ECM, extracellular matrix; GO, glyoxal; GLA, glycolaldehyde; MGO, methylglyoxal; PM, pyridoxamine; RNase, bovine pancreatic ribonuclease A.

10.1021/bi701190s CCC: $40.75
Published on Web 12/28/2007

Scheme 1

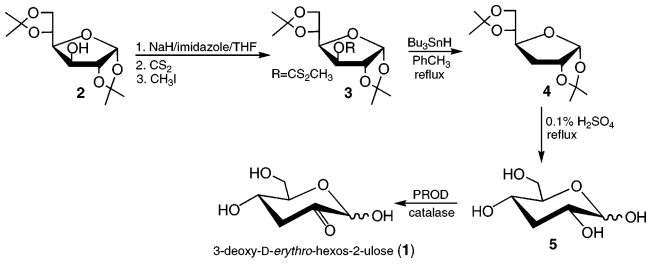

protein lysine and arginine residues (*23*−*25*). However, it is unknown whether these modifications by 3-DG are sufficient to affect protein functionality. As a nucleophile, PM can potentially scavenge 3-DG and inhibit protein modification, but these potential reactions between PM and 3-DG have not been investigated.

In the present study, we set out to establish whether 3-DG can cause functional protein damage and whether PM can protect proteins from this damage by 3-DG. Since the mode of PM scavenging depends on the nature of carbonyl species, it was also important to determine the specific mechanism of PM protection against 3-DG-induced damage if observed. We have demonstrated that 3-DG inhibits the activity of a model protein, RNase A, and modifies collagen IV, diminishing adhesion of renal mesangial cells to this major component of the extracellular matrix. Disruption of renal cell−matrix interactions suggests a pathogenic pathway by which 3-DG causes diabetic complications such as diabetic nephropathy. We have shown that PM ameliorated 3-DG-induced protein damage via a mechanism that includes transient reversible adduction of 3-DG by PM followed by irreversible PM-mediated oxidative cleavage of 3-DG to give nonreactive products.

MATERIALS AND METHODS

Materials. Pyridoxamine dihydrochloride, lanthanum nitrate hexahydrate, N^{α}-acetyl-L-lysine, N^{α}-acetyl-L-arginine, yeast RNA, and mouse type IV collagen isolated from EHS tumor were purchased from Sigma-Aldrich. Bovine pancreatic RNase A was obtained from Worthington Biochemical (Freehold, NJ).

*Synthesis of 3-Deoxy-*D*-erythro-hexos-2-ulose (**1**) (Scheme 1). 1,2;5,6-Di-O-isopropylidene-3-O-(methylthio)thiocarbonyl-*α*-D-glucofuranose (**3**) (26).* 1,2;5,6-Di-*O*-isopropylidene-α-D-glucofuranose (**2**; 5.20 g, 20.0 mmol) (*27*) was dissolved in THF (100 mL), imidazole (30 mg) was added, and then NaH (1.0 g, 40 mmol) was added batchwise. The reaction mixture was stirred for 1 h at room temperature under a nitrogen atmosphere. Carbon disulfide (6.0 mL, 100 mmol) was added, and the mixture was stirred for 2 h. Methyl iodide (3.0 mL, 48 mmol) was then added, and the mixture was stirred for an additional 1 h. The organic layer was washed with 1 M HCl, saturated $NaHCO_3$, and brine and dried over anhydrous Na_2SO_4. After evaporation of the solvent, the residue was crystallized ($EtOH/H_2O$) to afford the xanthate **3** (5.59 g, 80%).

*1,2;5,6-Di-O-isopropylidene-3-deoxy-*α*-*D*-glucofuranose (**4**) (28).* Compound **3** (3.5 g, 10 mmol) in toluene (60 mL) was added by a dropping funnel (1 drop every 2 s) to tri-*n*-butyltin hydride (TBTH; 4.0 g) in toluene (50 mL) under N_2 and at reflux. Refluxing was continued overnight, and the solvent was removed with a rotary evaporator. Acetonitrile (40 mL) and hexane (40 mL) were added to the residue, and the two-phase solution was stirred vigorously for 15 min. The lower acetonitrile layer was then separated, and the hexane phase was washed with acetonitrile (15 mL). Extraction of the combined acetonitrile solutions was repeated twice. The combined acetonitrile phase was concentrated to give product **4** (2.05 g, 84%).

*3-Deoxy-*D*-ribo-hexose (3-Deoxy-*D*-glucose) (**5**).* Compound **4** (2.0 g, 8.2 mmol) was dissolved in 0.1% (v/v) aqueous H_2SO_4 (120 mL), and the reaction mixture was refluxed for 1 h in an oil bath. After cooling, the solution was treated with Dowex 1 × 8 (HCO_3^-) ion-exchange resin to adjust the pH to ∼7, the resin was removed by filtration, and the solution was concentrated at 30 °C in vacuo to give **5** (1.14 g, 85%).

*3-Deoxy-*D*-erythro-hexos-2-ulose (3-Deoxy-*D*-glucosone) (**1**).* Bioconversion of **5** with pyranose 2-oxidase (glucose 2-oxidase, PROD, EC 1.1.3.10; Sigma) (*29*) was performed in a 1000 mL three-neck flask with gentle stirring and with aeration (∼20 mL/min) through a porous sintered glass tube at 25 °C. **5** (500 mg, 3.05 mmol) was dissolved in deionized water (400 mL), and PROD (250 IU) and catalase (10 000 IU, 0.2 mg; Sigma) were added while the pH was maintained at 7.0 with periodic additions of 0.01 N NaOH. The pH stopped dropping and the reaction was complete after ∼5 h. The suspension and the soluble catalase were removed by membrane filtration (0.2 μm filter), and the filtrate was concentrated at 30 °C in vacuo. The solution was applied to a column (2.5 × 100 cm) containing Dowex 50 × 8 (200−400 mesh) ion-exchange resin in the Ca^{2+} form (*30*). The column was eluted with distilled, decarbonated water at ∼1.5 mL/min, and fractions (12 mL) were collected and assayed by TLC (silica gel, spots detected by charring after spraying with 1% (w/v) $CeSO_4$−2.5% (w/v) $(NH_4)_6Mo_7O_{24}$−10% aqueous H_2SO_4 reagent) (*31*). Fractions 24−29, which contained osone **1**, were pooled and concentrated at 30 °C in vacuo. The product (489 mg, 3.0 mmol, 98%) was stored as an aqueous solution (∼50 mL) at 4 °C.

*^{13}C-Labeled 3-Deoxy-*D*-glucosone (**1**).* 3-Deoxy-D-[1-^{13}C]-glucosone and 3-deoxy-D-[2-^{13}C]glucosone were prepared as described for the unlabeled compound but substituting 1,2;5,6-di-*O*-isopropylidene-α-D-[1-^{13}C]glucofuranose and 1,2;5,6-di-*O*-isopropylidene-α-D-[2-^{13}C]glucofuranose, respectively, in the syntheses. The ^{13}C-labeled isopropylidene derivatives were prepared from D-[1-^{13}C]glucose and D-[2-^{13}C]glucose obtained from Omicron Biochemicals, Inc. (South Bend, IN).

Cell Culture. Conditionally immortalized mouse mesangial cells were kindly provided by Dr. Ambra Pozzi, Vanderbilt University Medical Center, Nashville, TN (*32*). The mesangial cells were propagated in DMEM medium supplemented with 10% FBS, 100 U/mL penicillin, 100 μg/mL streptomycin, and 100 U/mL interferon-γ at 33 °C. For differentiation, the cells were cultured in the above medium without interferon-γ at 37 °C. Low passages (<15) of the immortalized cells were used to ensure the preservation of the specific properties characteristic of the differentiated state (*32*).

Cell Adhesion Assay. Cell adhesion was quantified using crystal violet staining as previously described (*33*).

Modification of Collagen IV. Collagen IV was immobilized on 96-well plates (Nunc, Rochester, NY) in TBS buffer at

4 °C overnight as described earlier (*34*). The plates were washed twice with 200 mM sodium phosphate buffer, pH 7.5, and incubated in the same buffer with or without additives in the wet chamber to prevent changes in the sample volume due to evaporation; 0.02% sodium azide was added to suppress bacterial growth. Incubation buffers were replaced daily with the corresponding fresh buffer solutions to maintain steady-state concentrations of additives. All incubations were carried out in the dark at 37 °C. There was no detectable collagen IV desorption in any of the treatments over the course of the experiment as measured by the alkaline phosphatase (AP) competition assay (*35*) (data not shown).

The AP competition assay was validated by measuring desorption of the recombinant α3NC1 domain of collagen IV. The protein was modified with 1 mM MGO as previously described (*34*). Along with the use of AP competition assay, protein desorption was also determined by measuring bound protein by ELISA using either specific Goodpasture antibodies (*36*) or anti-FLAG antibody (Sigma-Aldrich), and by measuring unbound protein in the incubation buffer using LC−MS as described earlier (*34*). No desorption of either modified or unmodified protein was detected by any of the methods (data not shown).

Measurements of RNase Activity. RNase activity was determined by measuring the formation of acid-soluble oligonucleotide (*37*), with some modifications as previously described (*11*). For the assay, 100 μL of 3 μg/mL RNase in 100 mM sodium acetate, pH 5.0, was mixed with 100 μL of 1% yeast RNA in the same buffer. After the incubation at 37 °C for 5 min, the reaction was stopped by the addition of 100 μL of an ice-cold solution of 0.8% lanthanum nitrate in 18% perchloric acid. The incubation tubes were kept on ice for 5 min to ensure complete precipitation of undigested RNA and then centrifuged at 12000*g* for 10 min. An aliquot of the supernatant (20 μL) was diluted to 1 mL with distilled water, and the amount of digested (solubilized) RNA was determined by measuring the absorbance at 260 nm. The activity of RNase incubated either alone or with PM at 37 °C was monitored separately and used as the reference for each incubation time. This reference activity did not change significantly over the course of incubation.

Determination of Free Amino Groups. These determinations were performed according to the TNBSA assay protocol (Pierce). The reaction mixture was diluted (1:100, v/v) with 0.1 M sodium bicarbonate buffer, pH 8.5. An aliquot (0.25 mL) of 0.01% (w/v) TNBSA was added to 0.5 mL of sample. After the incubation at 37 °C for 2 h, 0.25 mL of 10% SDS and 0.125 mL of 1 N HCl were added to each sample, and the absorbance was recorded at 335 nm.

HPLC Analysis. HPLC analyses were performed using a Waters HPLC system equipped with a Shimadzu RF-551 spectrofluorimetric detector and Supelcosil LC318 (4.6 × 250 mm, 5 μm) HPLC column (Supelco, PA). Solvent A was 0.1% heptafluorobutyric acid in water, and solvent B was 75% acetonitrile in water; the flow rate was 1 mL/min. The following gradient program was used: 0−5 min, 5% B; 5−25 min, linear gradient to 100% B; 25−30 min, 100% B; 30−31 min, linear gradient to 5% B. Under these conditions PM eluted at 15.5 min.

Mass Spectrometry. MS analyses were performed using a Finnigan TSQ-7000 (San Jose, CA) triple-quadrupole mass spectrometer equipped with a standard API-1 electrospray ionization source outfitted with a 100 μL i.d. deactivated fused silica capillary. Nitrogen gas was used for the sheath gas at a pressure of 65 psi. The spectrometer was operated in the positive ion mode, and the electrospray needle was maintained at 4.5 kV. The heated capillary was operated at 20 V and 200 °C, and the tube lens voltage was set at 79.5 V. The samples were introduced using a Harvard Apparatus model 22 syringe pump operating at a flow rate of 10 μL/min. Prior to injection, the samples were diluted 100-fold with acetonitrile. Full-scan spectra were acquired in the *m*/*z* range of 150−750 at a rate of 1 scan/s.

NMR Spectroscopy. NMR spectra of 3-DG ± PM reaction mixtures (90:10 H_2O/D_2O) were obtained at 30 °C on a Varian Unity*Plus* FT-NMR spectrometer operating at 599.887 MHz for ^1H and 150.854 MHz for ^{13}C. The samples were analyzed in 3 mm NMR tubes using a dual $^{13}C/^1H$ microprobe (Nalorac), and the chemical shifts were referenced externally to sodium 4,4-dimethyl-4-silapentane-1-sulfonate (DSS).

^1H NMR spectra were collected with an 8000 Hz spectral window and a ∼2.1 s recycle time. FIDs were zero-filled to give final digital resolutions of <0.05 Hz/point. $^{13}C\{^1H\}$ NMR spectra were collected with ∼36 000 Hz spectral windows and ∼5.8 s recycle times. ^1H-decoupled ^{13}C NMR spectra without NOE were obtained with ∼36 000 Hz spectral windows and ∼18 s recycle times. To suppress heteronuclear $^{13}C-^1H$ NOE, ^1H decoupling was applied only during data acquisition (gated decoupling). All ^{13}C FIDs were processed to optimize spectral S/N (LB = 1) and to yield digital resolutions of ∼0.14 Hz/point. ^{13}C signal assignments were made via 2D HMQC spectra. $^1H-^1H$ and $^{13}C-^1H$ *J* couplings are reported in hertz and are accurate to ±0.1 Hz unless otherwise indicated.

Statistical Analysis. Data were expressed as the mean ± SD, and statistical analysis was performed using Student's *t* test. Differences were considered statistically significant if *p* values were <0.05.

RESULTS

Inhibition of RNase Activity by 3-DG and Protection by PM. RNase is one of the classical model proteins used in studies of protein glycation. RNase activity can be inhibited by glucose and by the reactive carbonyl species GO and GLA (*11*, *38*), most likely due to modification of Lys^7 and Lys^{41} in the substrate binding site of the enzyme (*38*). 3-DG significantly inhibited RNase activity in a time- and concentration-dependent manner (Figure 1), and PM protected the enzyme from inhibition by 3-DG (Figure 1). At equimolar concentrations, PM was more effective at protecting RNase activity compared to N^{α}-acetyl-L-lysine or N^{α}-acetyl-L-arginine (Figure 1B).

Inhibition of Cell−Matrix Interactions by 3-DG and Protection by PM. Previous studies have found elevated levels of 3-DG in diabetic plasma and detected 3-DG-derived protein modifications in renal tissues of diabetic patients (*13*, *14*, *17*). We hypothesized that modifications of long-lived renal matrix proteins by 3-DG contribute to perturbation of cell−matrix interactions in diabetes.

Purified collagen IV, a major component of glomerular mesangial matrix, was modified with 3-DG for 30−60 days. The microplate well coverage was >97%, and no protein

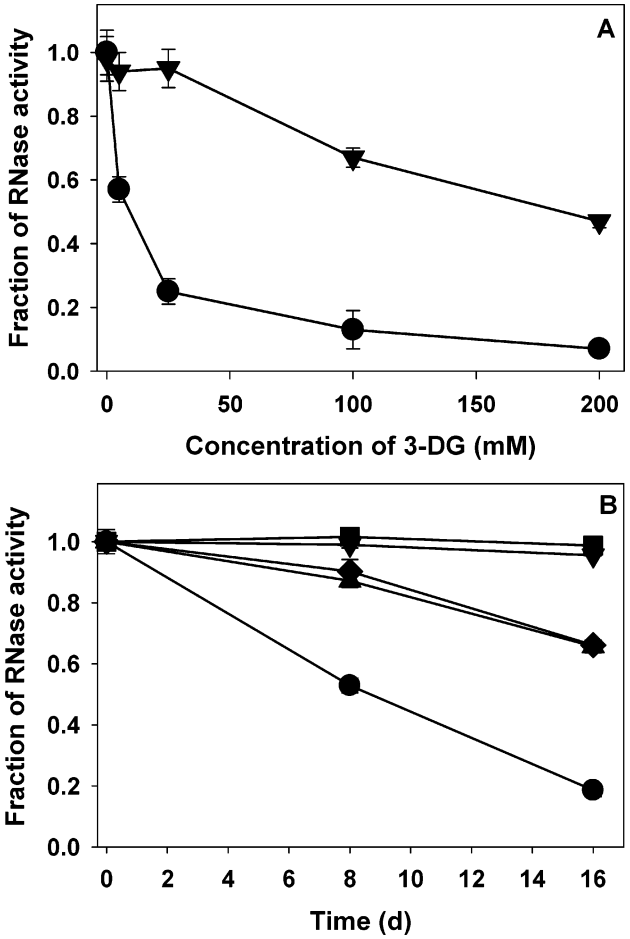

FIGURE 1: Inactivation of RNase by 3-DG and protection by PM. (A) Effect of 3-DG concentration on RNase activity after 16 days of incubation without PM (circles) and with 15 mM PM (triangles). (B) Time course of RNase activity. RNase was incubated alone (squares), with 25 mM 3-DG (circles), or with 3-DG and the following additives (15 mM): PM (triangles), *N*-acetyllysine (inverted triangles), or *N*-acetylarginine (tilted squares). The incubations were carried out at 37 °C in 200 mM sodium phosphate buffer with 0.02% sodium azide, pH 7.5. The RNase concentration was 1 mg/mL. The RNase activity was determined as described in the Materials and Methods. Each symbol represents the mean ± SD ($n = 3$). PM, *N*-acetyllysine, or *N*-acetylarginine did not affect the RNase activity after 16 days of incubation (data not shown).

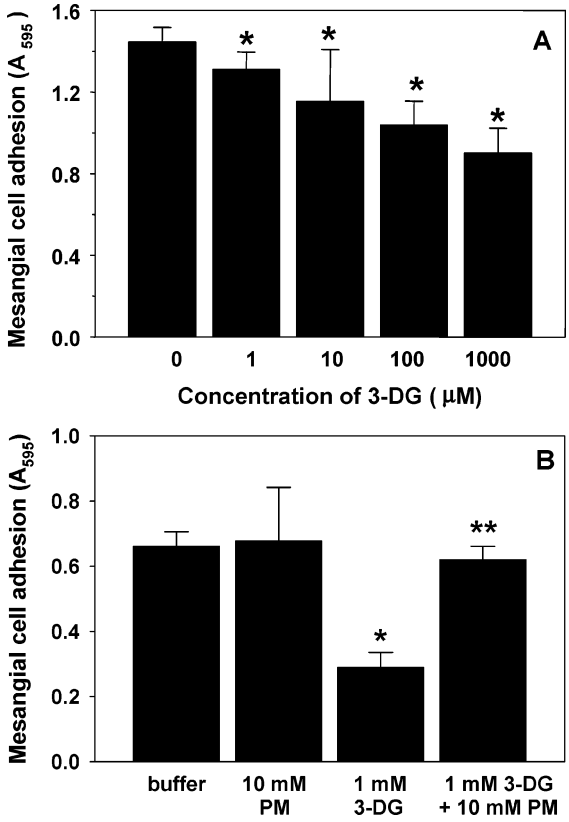

FIGURE 2: Inhibition of mesangial cell adhesion to 3-DG-modified collagen IV and protective effect of PM. Plates (96-well) were coated with EHS collagen IV (20 μg/mL) and incubated in 200 mM sodium phosphate buffer (200 μL) containing 0.02% sodium azide, pH 7.5, at 37 °C. For the treatment, the buffer was supplemented with the indicated concentrations of either 3-DG or PM alone or with 3-DG and PM as described in the Materials and Methods. After extensive washing, the adhesion of mesangial cells to collagen IV was measured as described in the Materials and Methods. Incubations were carried out for either 30 (A) or 60 (B) days. Key: *, differences vs unmodified protein are significant ($p < 0.05$, $n = 4$); **, difference *vs* 3-DG-modified protein is significant ($p < 0.05$, $n = 4$).

desorption was detected after different treatments as determined by alkaline phosphatase competition assay (*35*) (data not shown). These incubation times are relatively short compared to the collagen IV physiological half-life of ~2 years (*39*). Nevertheless, modification of collagen IV with 3-DG caused significant inhibition of mesangial cell adhesion to this protein (Figure 2A). Importantly, the effect was significant at 1 μM 3-DG (Figure 2A), a concentration comparable to reported 3-DG plasma levels of ~0.5 μM in diabetes (*13*). PM ameliorated 3-DG-induced inhibition of mesangial cell adhesion (Figure 2B). A 10-fold molar excess of PM over 3-DG in this experiment reflected the fact that in vivo the therapeutic PM concentration is significantly higher than the concentration of 3-DG (*2*, *13*).

Mechanism of 3-DG Detoxification by PM. We hypothesized that PM protection from 3-DG-induced protein damage is caused by direct scavenging of 3-DG by PM. Reactive PM amino groups were lost in the presence of 3-DG, consistent with possible adduct formation (Figure 3A), and reaction product(s) of PM and 3-DG were detected by reversed-phase HPLC (Figure 3B). ESI-MS analysis of the reaction mixture detected new products with molecular masses corresponding to 3-DG−PM adducts as shown in Figure 4.

Reaction of Unlabeled 3-DG with PM. Aqueous solutions of 3-DG contain multiple forms in equilibrium (*40*, *41*), giving rise to complex ^{1}H (600 MHz) and ^{13}C (150 MHz) NMR spectra. Unexpectedly, ^{1}H and ^{13}C NMR spectra of solutions resulting from the reaction of 3-DG with PM at 37 °C, each at 10 mM, for 30 days were relatively simple (Figures 5 and 6) and indicated the formation of one major product. Analysis of the ^{1}H NMR spectrum showed that the C3−C6 fragment of 3-DG remained intact in the product (Figure 5B), on the basis of the internally consistent $^2J_{HH}$ and $^3J_{HH}$ values measured from the spectrum (Table 1). The 2D ^{13}C−^{1}H HMQC spectrum (Figure S1, Supporting Information) showed that the major ^{1}H signals correlated with the major signals observed in the ^{13}C{^{1}H} spectrum (Figure 6A). Using these data, several potential reaction products were eliminated from consideration, including a family of structures (**6**−**11**) generated via direct adduct formation between 3-DG and PM (Scheme S1, Supporting Informa-

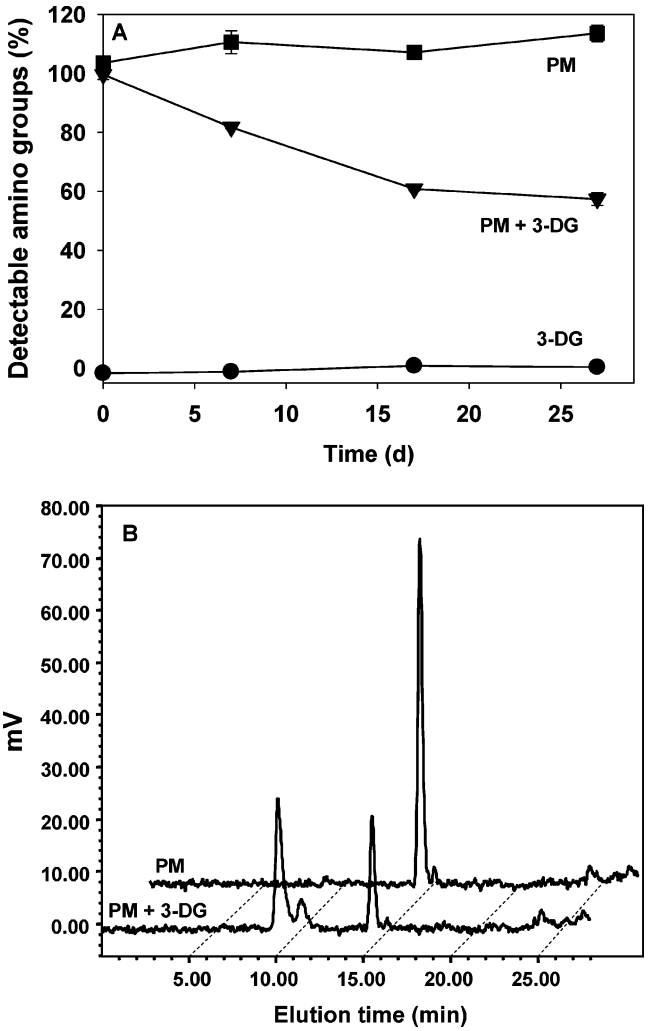

FIGURE 3: Reaction between 3-DG and PM. Pyridoxamine and 3-DG (10 mM each) were incubated at 37 °C in the dark in 200 mM sodium phosphate buffer with 0.02% sodium azide, pH 7.5. (A) The loss of reactive PM amino groups was measured using the TNBSA method as described in the Materials and Methods. Each symbol represents the mean ± SD, $n = 3$. (B) After 14 days of incubation, the reaction mixtures were analyzed using ion pair RP-HPLC as described in the Materials and Methods.

tion). Likewise, one of the transamination products (**12**; Scheme S2, Supporting Information) was inconsistent with the NMR results. The structure of the major reaction product was determined through selective ^{13}C-labeling studies.

Reaction of ^{13}C-Labeled 3-DG with PM. NMR studies were conducted with 3-DG labeled with ^{13}C at either C1 or C2, since data obtained from reactions involving unlabeled 3-DG indicated that the C3−C6 fragment of 3-DG remained intact, implying that structural changes occurred at C1 and C2. Reaction mixtures containing ^{13}C-labeled 3-DG with (3-DG + PM) and without (3-DG − PM) PM were incubated for 30 days, and samples were withdrawn periodically for analysis by ^{13}C NMR.

The ^{13}C{^{1}H} NMR spectrum of the [1-^{13}C]-3-DG + PM reaction mixture contained four labeled signals at 184.36, 183.71, 173.66, and 147.01 ppm (Figure 7A). In the [1-^{13}C]-3-DG − PM reaction mixture, the signals at 184.36 and 183.71 ppm were dominant (Figure 7B). The signal at 173.66 ppm appeared as a doublet in the ^{1}H-coupled ^{13}C NMR spectrum, indicating a monoprotonated carbon with $^{1}J_{CH}$ = 194.8 Hz (data not shown). ^{1}H and ^{13}C NMR spectra of authentic sodium formate gave an identical carbon chemical shift and $^{1}J_{CH}$ = 194.7 Hz. ^{1}H and ^{13}C NMR spectra of the unlabeled 3-DG + PM reaction mixture (Figures 5 and 6) contained signals consistent with the presence of formate (signal "a" in Figure 5A, signal "b" in Figure 6A). It is noteworthy that the signal at 173.66 ppm in Figure 6B is a doublet with the same $^{1}J_{CH}$ observed for authentic sodium formate. Detection of [^{13}C]formate in [1-^{13}C]-3-DG + PM reaction mixtures suggests C1−C2 bond cleavage in 3-DG, with C1 appearing as the formate carbon. This cleavage reaction appears less favored in solutions of [1-^{13}C]-3-DG alone, as indicated by the presence of a relatively weak formate signal and the presence of two major products with ^{13}C labeling at carboxylate (COOH) carbons (Figure 7B). The latter products result from direct structural rearrangement of the [1-^{13}C]-3-DG carbon skeleton (see below).

The above interpretation of the [1-^{13}C]-3-DG + PM NMR data was tested by studying the reaction with [2-^{13}C]-3-DG. The ^{13}C{^{1}H} NMR spectrum of a solution of [2-^{13}C]-3-DG − PM after 30 days contained two paired ^{13}C-labeled signals at 73.36 and 71.95 ppm and a weak ^{13}C-labeled signal at 182.90 ppm (Figure 8B). The same signals were observed in the [2-^{13}C]-3-DG + PM reaction mixture, but that at 182.90 ppm was considerably more intense than those at 73.36 and 71.95 ppm (Figure 8A). The ^{1}H-coupled ^{13}C NMR spectrum of the same reaction mixture showed the 71.95 ppm signal split into a doublet ($^{1}J_{CH}$ = ∼145.9 Hz), indicative of a secondary alcoholic carbon, whereas the signal at 182.90 ppm, indicative of a COOH carbon, appeared as eight lines (ddd) containing three long-range J_{CH} values (absolute values): 3.0, 5.8, and 6.5 Hz. This multiplicity suggested that the labeled COOH carbon is two and three bonds removed from a CH_2 group and a CH group, respectively; that is, the coupling data are consistent with a ^{13}COOH−CH_2−CHOH− fragment.

Integration of signals in the ^{13}C NMR spectra of [1-^{13}C]- and [2-^{13}C]-3-DG reaction mixtures indicates that, in the absence of PM, 3-DG spontaneously converts primarily to the two C2-epimeric 3-deoxyhexonic acids (metasaccharinic acids) 3-deoxy-D-*ribo*-hexonic acid (**13**) and 3-deoxy-D-*arabino*-hexonic acid (**14**) via the addition of water. One

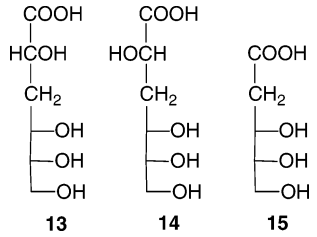

epimer is highly favored, and preparation of authentic **13** (see the Supporting Information) showed that **14** is the more abundant product. In the presence of PM, however, 3-DG follows a C1−C2 oxidative cleavage pathway, generating HCOOH from C1 and a COOH functional group at C2. Since analysis of the ^{1}H NMR spectrum of unlabeled 3-DG + PM reactions showed the C3−C6 fragment of 3-DG remains intact during the reaction, the primary C1−C2 cleavage product was postulated to be 2-deoxy-D-*erythro*-pentonic acid (2-deoxy-D-ribonic acid) (**15**). This prediction was confirmed by preparing authentic sodium 2-deoxy-D-ribonate by bro-

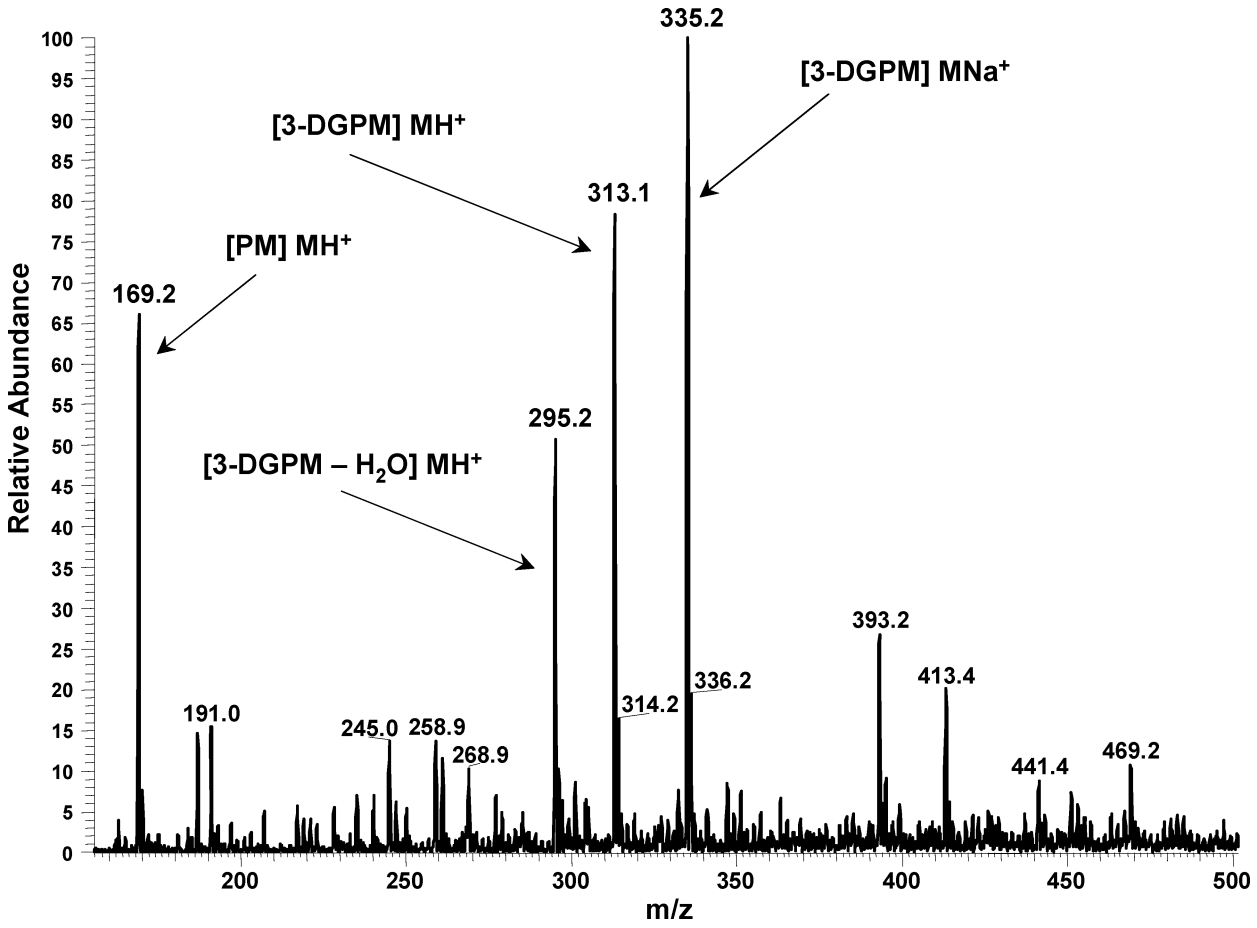

FIGURE 4: Mass spectrometric detection of 3-DG-PM adducts. Pyridoxamine and 3-DG (10 mM each) were incubated in the dark in 200 mM sodium phosphate buffer with 0.02% sodium azide, pH 7.5, at 37 °C for 14 days. The reaction mixture was analyzed using direct infusion ESI-MS as described in the Materials and Methods.

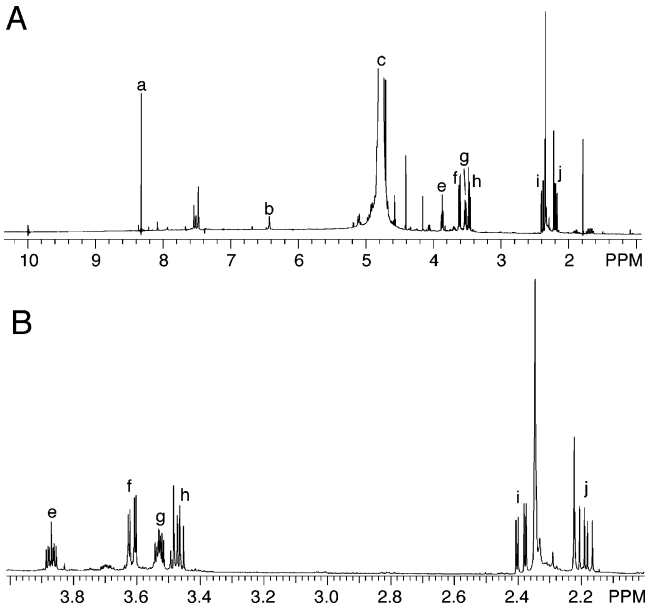

FIGURE 5: (A) ^{1}H NMR spectrum (600 MHz) of a 3-DG + PM reaction mixture after 30 days at 37 °C. Signal c arises from residual solvent HOD. Signals e−j are attributed to the major product. Signal b may be due to pyridoxal hydrate. (B) Expansion of the major product signals e−j shown in (A), showing signal multiplicities from which $^{2}J_{HH}$ and $^{3}J_{HH}$ values were measured (Table 1).

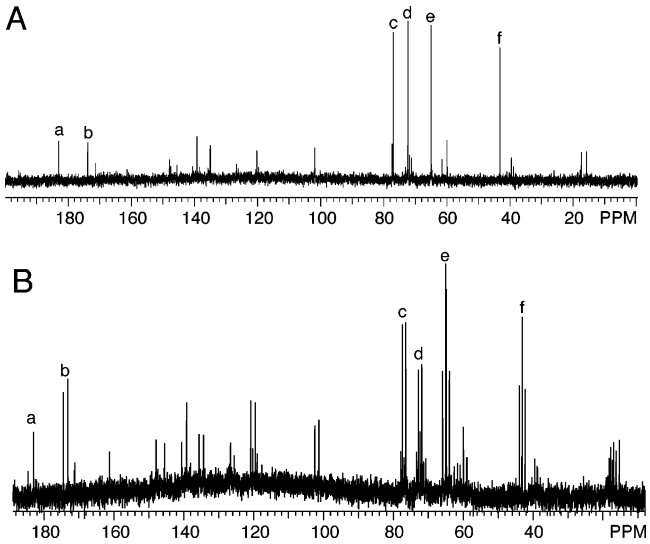

FIGURE 6: (A) ^{13}C{^{1}H} NMR spectrum (150 MHz) of a 3-DG + PM reaction mixture after 30 days at 37 °C. Signals a and c−f are attributed to the major reaction product. Chemical shifts are given in Table 1. The signal at ∼102 ppm may be due to pyridoxal hydrate. (B) ^{1}H-coupled ^{13}C NMR spectrum of the same 3-DG + PM reaction mixture analyzed in (A). Multiplicities of the major signals are given in Table 1.

mine oxidation of 2-deoxy-D-ribose (see the Supporting Information). Signals in its ^{1}H and ^{13}C NMR spectra matched the predominant signals shown in Figures 5 and 6.

^{13}C NMR spectra shown in Figures 6A, 7A, and 8 were obtained on labeled 3-DG reaction mixtures in a ^{1}H-decoupled + NOE mode (^{13}C{^{1}H}). Since the relaxation and heteronuclear NOE properties of protonated (e.g., CH) and

Table 1: Interpretation of the Major ^{1}H and ^{13}C NMR Signals Observed in Unlabeled 3-DG−PM Reaction Mixtures

^{1}H signal[a] (ppm)	J_{HH}[b] (Hz)	^{1}H signal assignment[c]	carbon signal correlations[d,e] (ppm)
3.85	3.8, 5.6, 9.4	H4	72.33 (d)
3.57	3.2, −11.6	H6	65.05 (t)
3.49	3.2, 5.6, 7.2	H5	77.01 (d)
3.42	7.2, −11.6	H6	65.05 (t)
2.34	3.8, −15.1	H3	43.08 (t)
2.14	9.4, −15.1	H3	43.08 (t)

[a] Predominant ^{1}H signals observed in unlabeled 3-DG−PM reaction mixtures, pH 7.5, 37 °C, relative to the peak for external DSS. [b] J_{HH} values extracted from the corresponding ^{1}H signal multiplets. [c] Assignments based on the C1−C6 carbons of 3-DG (the C3−C6 fragment remains intact in the major product). [d] Correlations observed in the 2D ^{13}C−^{1}H HMQC spectrum. [e] ^{1}H-coupled ^{13}C data gave doublets (d) or triplets (t) for the indicated signals, indicating CH and CH_2 groups, respectively.

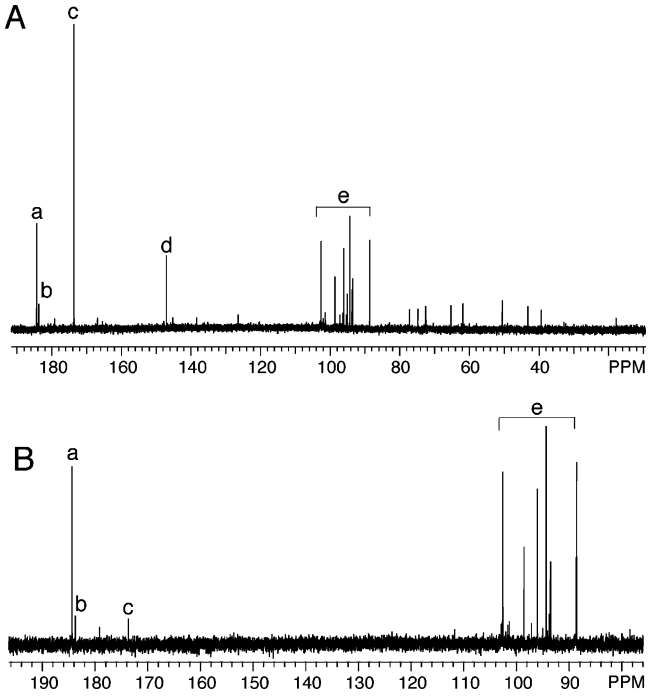

FIGURE 7: (A) ^{13}C{^{1}H} NMR spectrum of a [1-^{13}C]-3-DG + PM reaction mixture after 30 days at 37 °C. Signals a−e arise from labeled species, and the weaker signals from 40 to 80 ppm are natural abundance signals from PM and 3-DG. Signals e are primarily from unreacted [1-^{13}C]-3-DG. (B) ^{13}C{^{1}H} NMR spectrum of [1-^{13}C]-3-DG after 30 days at 37 °C (no PM). Signals a−c and e match the corresponding signals in (A).

unprotonated (e.g., COOH) carbons differ, the relative intensities of labeled signals in these spectra give erroneous relative concentrations. Re-examination of the [2-^{13}C]-3-DG + PM (30 days) reaction mixture by ^{13}C NMR with ^{1}H decoupling − NOE showed the signal at 182.90 ppm significantly more intense than those at 71.95 and 73.36 ppm (Figure S2, Supporting Information), consistent with **15** being the major reaction product as indicated from NMR studies of unlabeled 3-DG reaction mixtures (Figures 5 and 6).

A second possible transamination product, 1-amino-1-deoxy-3-deoxy-D-fructose (**16**) (Scheme S1), was eliminated as the major product through synthesis of a structural analogue, 3-deoxy-D-fructose. ^{1}H and ^{13}C spectra of the latter did not match those obtained on unlabeled 3-DG + PM reaction mixtures, although weak signals in the latter ^{1}H

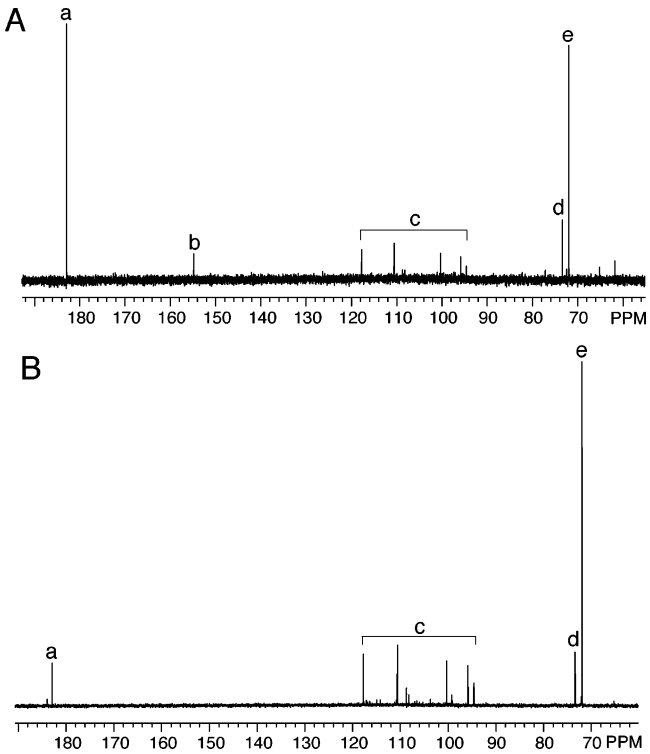

FIGURE 8: (A) ^{13}C{^{1}H} NMR spectrum of a [2-^{13}C]-3-DG + PM reaction mixture after 30 days at 37 °C. Signals a−e arise from labeled species. Signals c are primarily from unreacted [2-^{13}C]-3-DG. (B) ^{13}C{^{1}H) NMR spectrum of [2-^{13}C]-3-DG after 30 days at 37 °C. Signals a and c−e match the corresponding signals in (A).

spectra indicated the possible presence of aminofructose at very low levels.

^{13}C NMR spectra of the [1-^{13}C]-3-DG + PM and [2-^{13}C]-3-DG + PM reaction mixtures contained minor labeled signals at 147.01 and 154.80 ppm, respectively (Figures 7 and 8). While the structures responsible for these signals were not identified, potential candidates include those produced from a reaction of two PM and two 3-DG molecules analogous to that reported for methylglyoxal (Scheme S2) (*9*). A byproduct of this reaction is 2-deoxy-D-ribonate **15**, and thus, **15** observed in 3-DG + PM reaction mixtures may derive from this secondary pathway in addition to the primary direct degradation of **1** via oxidative cleavage.

DISCUSSION

Diabetes is characterized by the elevated levels of reactive carbonyl compounds, a phenomenon known as "carbonyl stress" (*42*). Chemical modification of tissue proteins by these compounds has been documented in both diabetic patients and animal models of diabetes, including modification of arginine residues by MGO and 3-DG (*15*, *17*, *43*, *44*). These arginine modifications may affect protein function as has been shown for MGO-modified mitochondrial proteins in diabetic rats (*45*).

More recently, a potential pathogenic mechanism involving disruption of integrin-mediated cell−matrix interactions by MGO via modification of specific arginine residues in long-lived proteins of the extracellular matrix has been demonstrated using several different cell types in culture (*34*, *46*, *47*). It has been demonstrated that dicarbonyl compounds form adducts with arginine residues within specific integrin binding sites (*34*, *46*, *47*) and affect integrin binding (*34*),

while modification of lysine residues is not mechanistically important (*34*, *47*). These findings provided a potential mechanistic connection between "carbonyl stress" and diabetic lesions such as mesangial expansion and podocyte detachment. We demonstrate here that a structurally different reactive carbonyl compound, 3-DG, also perturbs cell−matrix interactions at physiologically relevant concentrations and within a relatively short time. Thus, 3-DG, along with MGO, may contribute to pathogenesis of diabetic nephropathy via perturbation of renal cell−matrix interactions. Since PM scavenges both MGO (*9*) and 3-DG (this paper), we propose that the therapeutic effect of PM in diabetic nephropathy is achieved, in part, via protection of long-lived matrix proteins from modification by reactive carbonyl compounds, thus preserving critical cell−matrix interactions in the kidney.

In PM therapy in vivo, the reaction of toxic carbonyl compounds with PM would be favored because of the significant molar excess of PM (up to 100 μM (*2*)) over free reactive carbonyl species (0.5−2 μM (*13*)). Thus, the plasma concentration of PM is sufficient for scavenging the major reactive carbonyl species, including 3-DG. Clearly, the efficacy of PM in vivo will be influenced by factors such as the nature of carbonyl species, local tissue concentrations of reactive carbonyls and PM, and the concentration of endogenous carbonyl scavengers. However, even very small amounts of reactive carbonyls that exceed the capacity of endogenous carbonyl scavenger systems may lead, over a long time, to an increase in the modification of critical arginine residues in long-lived matrix proteins. By trapping the excess reactive carbonyls, PM may provide a significant protective effect. Our data suggest that PM can effectively compete for 3-DG with protein lysine and arginine side chains (Figure 1B) and, thus, protect these protein residues from modification. Moreover, since the hydroimidazolone adducts between arginine residues and reactive carbonyl species are metastable (*48*), the depletion of excess free reactive carbonyls may lead to gradual depletion of arginine adducts in ECM proteins and improvement of cell−matrix interactions.

Mechanistic studies by ^{13}C NMR using ^{13}C-labeled 3-DG have shown that 3-DG degrades in aqueous solution either via skeletal rearrangement or via backbone oxidative cleavage pathways and that the latter pathway is favored in the presence of PM. Studies of selectively ^{13}C-labeled 3-DG demonstrate that two C2-epimeric C_6 metasaccharinic acids are produced from 3-DG spontaneously in the absence of PM after 30 days, with an unequal distribution of both epimers (Scheme 2). When PM is present, however, the same skeletal rearrangement occurs, but a competing oxidative cleavage pathway becomes highly favored. In the presence of PM, oxidative cleavage of the C1−C2 bond of 3-DG is favored, yielding formate anion (from C1) and 2-deoxy-D-ribonate (Scheme 2). The precise chemical mechanisms responsible for this cleavage reaction are unclear. It is possible that either formaldehyde and/or 2-deoxy-D-ribose are intermediates and that metal ions, present endogenously in the phosphate buffer, are required for the oxidation.

The present results suggest a potential role for PM in promoting C1−C2 bond oxidative cleavage, possibly by complexing 3-DG to give transient adducts having structures similar to those shown in Scheme S1. The protection afforded

Scheme 2

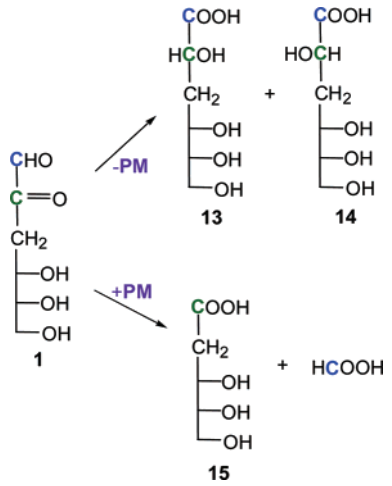

by PM in reactions of 3-DG with proteins may involve two steps, namely, transient adduct formation which presumably scavenges 3-DG from solution in a rapid and reversible fashion (Figures 3 and 4 and Scheme S1), followed by a second slower irreversible oxidative step to give the nonreactive aldonate (Figures 5−8 and Scheme 2). Our observation that PM provides significant protection of RNase activity even at a high 3-DG-to-PM molar ratio (Figure 1B) is consistent with this mechanism. Although PM can participate in nonenzymatic transamination reactions (*49*), our results do not support the presence of an alternative nonenzymatic transamination mechanism for the scavenging reaction between PM and 3-DG.

PM has demonstrated therapeutic effects in clinical trials for diabetic nephropathy (*1*). However, the mechanism(s) of PM action is poorly understood. PM can potentially protect proteins from diabetes-induced chemical modification via several mechanisms, including sequestration of redox-active metal ions, scavenging of hydroxyl radical, and scavenging of reactive carbonyl species (reviewed in ref *6*). PM may also act as a precursor of pyridoxal 5′-phosphate (PLP), an active form of vitamin B_6. It has been shown that pyridoxine, a major physiological precursor of PLP, can rapidly normalize endothelial dysfunction in children with type I diabetes (*50*). The mechanism of this effect is unknown and may include vitamin B_6 action as a coenzyme as well as protection of protein amino groups at potential glycation sites by PLP (*51*). PLP also inhibited peritoneal damage induced by glucose-based dialysate in rats; carbonyl scavenging by PLP was suggested as a possible mechanism (*52*). However, this mechanism is unlikely because PLP lacks a nucleophilic group.

In this paper, we propose a novel mechanism of PM protection against 3-DG toxicity involving transient adduction of 3-DG by PM followed by irreversible oxidative cleavage of 3-DG. This detoxification mechanism along with other carbonyl trapping mechanisms may contribute to the known therapeutic effect of PM in diabetic nephropathy. In particular, this therapeutic effect may derive from PM protection of extracellular matrix proteins and preservation of critical renal cell−matrix interactions.

ACKNOWLEDGMENT

We thank Dr. Ambra Pozzi for a generous gift of mouse glomerular mesangial cells.

SUPPORTING INFORMATION AVAILABLE

Figures and schemes showing the reaction mechanism between PM and 3-DG. This material is available free of charge via the Internet at http://pubs.acs.org.

REFERENCES

1. Williams, M. E. (2006) New potential agents in treating diabetic kidney disease: the fourth act, *Drugs 66*, 2287−2298.
2. Degenhardt, T. P., Alderson, N. L., Arrington, D. D., Beattie, R. J., Basgen, J. M., Steffes, M. W., Thorpe, S. R., and Baynes, J. W. (2002) Pyridoxamine inhibits early renal disease and dyslipidemia in the streptozotocin-diabetic rat, *Kidney Int. 61*, 939−950.
3. Stitt, A., Gardiner, T. A., Alderson, N. L., Canning, P., Frizzell, N., Duffy, N., Boyle, C., Januszewski, A. S., Chachich, M., Baynes, J. W., and Thorpe, S. R. (2002) The AGE inhibitor pyridoxamine inhibits development of retinopathy in experimental diabetes, *Diabetes 51*, 2826−2832.
4. Zheng, F., Zeng, Y. J., Plati, A. R., Elliot, S. J., Berho, M., Potier, M., Striker, L. J., and Striker, G. E. (2006) Combined AGE inhibition and ACEi decreases the progression of established diabetic nephropathy in B6 db/db mice, *Kidney Int. 70*, 507−514.
5. Tanimoto, M., Gohda, T., Kaneko, S., Hagiwara, S., Murakoshi, M., Aoki, T., Yamada, K., Ito, T., Matsumoto, M., Horikoshi, S., and Tomino, Y. (2007) Effect of pyridoxamine (K-163), an inhibitor of advanced glycation end products, on type 2 diabetic nephropathy in KK-A(y)/Ta mice, *Metabolism 56*, 160−167.
6. Voziyan, P. A., and Hudson, B. G. (2005) Pyridoxamine as a multifunctional pharmaceutical: targeting pathogenic glycation and oxidative damage, *Cell. Mol. Life Sci. 62*, 1671−1681.
7. Iacovella, G., Alderson, N. L., Chachich, M., Thorpe, S. R., and Baynes, J. W. (2003) Pyridoxamine decreases levels of reactive alpha-dicarbonyls in plasma of ZDF diabetic rats, *Diabetes 52*, A187.
8. Alderson, N. L., Chachich, M. E., Youssef, N. N., Beattie, R. J., Nachtigal, M., Thorpe, S. R., and Baynes, J. W. (2003) The AGE inhibitor pyridoxamine inhibits lipemia and development of renal and vascular disease in Zucker obese rats, *Kidney Int. 63*, 2123−2133.
9. Nagaraj, R. H., Sarkar, P., Mally, A., Biemel, K. M., Lederer, M. O., and Padayatti, P. S. (2002) Effect of pyridoxamine on chemical modification of proteins by carbonyls in diabetic rats: characterization of a major product from the reaction of pyridoxamine and methylglyoxal, *Arch. Biochem. Biophys. 402*, 110−119.
10. Metz, T. O., Alderson, N. L., Chachich, M. E., Thorpe, S. R., and Baynes, J. W. (2003) Pyridoxamine traps intermediates in lipid peroxidation reactions in vivo: evidence on the role of lipids in chemical modification of protein and development of diabetic complications, *J. Biol. Chem. 278*, 42012−42019.
11. Voziyan, P. A., Metz, T. O., Baynes, J. W., and Hudson, B. G. (2002) A post-Amadori inhibitor pyridoxamine also inhibits chemical modification of proteins by scavenging carbonyl intermediates of carbohydrate and lipid degradation, *J. Biol. Chem. 277*, 3397−3403.
12. Amarnath, V., Amarnath, K., Davies, S., and Roberts, L. J. 2nd (2004) Pyridoxamine: an extremely potent scavenger of 1,4-dicarbonyls, *Chem. Res. Toxicol. 17*, 410−415.
13. Odani, H., Shinzato, T., Matsumoto, Y., Usami, J., and Maeda, K. (1999) Increase in three alpha, beta-dicarbonyl compound levels in human uremic plasma: specific in vivo determination of intermediates in advanced Maillard reaction, *Biochem. Biophys. Res. Commun. 256*, 89−93.
14. Wells-Knecht, K. J., Lyons, T. J., McCance, D. R., Thorpe, S. R., Feather, M. S., and Baynes, J. W. (1994) 3-Deoxyfructose concentrations are increased in human plasma and urine in diabetes, *Diabetes 43*, 1152−1156.
15. Thornalley, P. J., Battah, S., Ahmed, N., Karachalias, N., Agalou, S., Babaei-Jadidi, R., and Dawnay, A. (2003) Quantitative screening of advanced glycation endproducts in cellular and extracellular proteins by tandem mass spectrometry, *Biochem. J. 375*, 581−592.
16. Niwa, T., Katsuzaki, T., Ishizaki, Y., Hayase, F., Miyazaki, T., Uematsu, T., Tatemichi, N., and Takei, Y. (1997) Imidazolone, a novel advanced glycation end product, is present at high levels in kidneys of rats with streptozotocin-induced diabetes, *FEBS Lett. 407*, 297−302.
17. Niwa, T., Katsuzaki, T., Miyazaki, S., Miyazaki, T., Ishizaki, Y., Hayase, F., Tatemichi, N., and Takei, Y. (1997) Immunohistochemical detection of imidazolone, a novel advanced glycation end product, in kidneys and aortas of diabetic patients, *J. Clin. Invest. 99*, 1272−1280.
18. Miyata, S., and Monnier, V. (1992) Immunohistochemical detection of advanced glycosylation end products in diabetic tissues using monoclonal antibody to pyrraline, *J. Clin. Invest. 89*, 1102−1112.
19. Szwergold, B. S., Howell, S., and Beisswenger, P. J. (2001) Human fructosamine-3-kinase: purification, sequencing, substrate specificity, and evidence of activity in vivo, *Diabetes 50*, 2139−2147.
20. Zyzak, D. V., Richardson, J. M., Thorpe, S. R., and Baynes, J. W. (1995) Formation of reactive intermediates from Amadori compounds under physiological conditions, *Arch. Biochem. Biophys. 316*, 547−554.
21. Thornalley, P. J., Langborg, A., and Minhas, H. S. (1999) Formation of glyoxal, methylglyoxal and 3-deoxyglucosone in the glycation of proteins by glucose, *Biochem. J. 344 Pt 1*, 109−116.
22. Thornalley, P. J., Yurek-George, A., and Argirov, O. K. (2000) Kinetics and mechanism of the reaction of aminoguanidine with the alpha-oxoaldehydes glyoxal, methylglyoxal, and 3-deoxyglucosone under physiological conditions, *Biochem. Pharmacol. 60*, 55−65.
23. Hayase, F., Nagaraj, R. H., Miyata, S., Njoroge, F. G., and Monnier, V. M. (1989) Aging of proteins: immunological detection of a glucose-derived pyrrole formed during Maillard reaction in vivo, *J. Biol. Chem. 264*, 3758−3764.
24. Dyer, D. G., Blackledge, J. A., Thorpe, S. R., and Baynes, J. W. (1991) Formation of pentosidine during nonenzymatic browning of proteins by glucose. Identification of glucose and other carbohydrates as possible precursors of pentosidine in vivo, *J. Biol. Chem. 266*, 11654−11660.
25. Biemel, K. M., Friedl, D. A., and Lederer, M. O. (2002) Identification and quantification of major Maillard cross-links in human serum albumin and lens protein. Evidence for glucosepane as the dominant compound, *J. Biol. Chem. 277*, 24907−24915.
26. Sanyal, A. K., and Purves, C. B. (1956) Some xanthate methyl esters of glucose, *Can. J. Chem. 34*, 426−435.
27. Schmidt, O. T. (1963) *Methods Carbohydr. Chem.*, Vol. 2, Academic Press, New York and London, p 318.
28. Barton, D. H. R., and McCombie, S. W. (1975) A new method for the deoxygenation of secondary alcohols, *J. Chem. Soc., Perkin Trans. 1*, 1574−1585.
29. Freimund, S., Huwig, A., Giffhorn, F., and Köpper, S. (1998) Rare keto-aldoses from enzymatic oxidation: substrates and oxidation products of pyranose 2-oxidase, *Chem.—Eur. J. 4*, 2442−2455.
30. Angyal, S., Bethell, G. S., and Beveridge, R. (1979) Complexes of carbohydrates with metal cation. 10. Separation of sugars and of polyols on cation-exchange resins in the calcium form, *Carbohydr. Res. 73*, 9−18.
31. Tropper, F. D., Andersson, F. O., Grand-Maitre, C., and Roy, R. (1992) Phase transfer catalyzed synthesis of 4-nitrophenyl 1-thio-β-D-glycobiosides, *Carbohydr. Res. 229*, 149−154.
32. Chen, X., Moeckel, G., Morrow, J. D., Cosgrove, D., Harris, R. C., Fogo, A. B., Zent, R., and Pozzi, A. (2004) Lack of integrin alpha1beta1 leads to severe glomerulosclerosis after glomerular injury, *Am. J. Pathol. 165*, 617−630.
33. Pedchenko, V., Zent, R., and Hudson, B. G. (2004) Alpha(v)-beta3 and alpha(v)beta5 integrins bind both the proximal RGD site and non-RGD motifs within noncollagenous (NC1) domain of the alpha3 chain of type IV collagen: implication for the mechanism of endothelia cell adhesion, *J. Biol. Chem. 279*, 2772−2780.
34. Pedchenko, V. K., Chetyrkin, S. V., Chuang, P., Ham, A. J., Saleem, M. A., Mathieson, P. W., Hudson, B. G., and Voziyan, P. A. (2005) Mechanism of perturbation of integrin-mediated cell-matrix interactions by reactive carbonyl compounds and its implication for pathogenesis of diabetic nephropathy, *Diabetes 54*, 2952−2960.
35. Steinitz, M., and Baraz, L. (2000) A rapid method for estimating the binding of ligands to ELISA microwells, *J. Immunol. Methods 238*, 143−150.
36. Saus, J., Wieslander, J., Langeveld, J. P., Quinones, S., and Hudson, B. G. (1988) Identification of the Goodpasture antigen

as the alpha 3(IV) chain of collagen IV, *J. Biol. Chem. 263*, 13374−13380.
37. Kalnitsky, G., and Resnick, H. (1959) The effect of an altered secondary structure on ribonuclease activity, *J. Biol. Chem. 234*, 1714−1717.
38. Watkins, N. G., Thorpe, S. R., and Baynes, J. W. (1985) Glycation of amino groups in protein. Studies on the specificity of modification of RNase by glucose, *J. Biol. Chem. 260*, 10629−10636.
39. Heikkila, P., Tibell, A., Morita, T., Chen, Y., Wu, G., Sado, Y., Ninomiya, Y., Pettersson, E., and Tryggvason, K. (2001) Adenovirus-mediated transfer of type IV collagen alpha5 chain cDNA into swine kidney in vivo: deposition of the protein into the glomerular basement membrane, *Gene Ther. 8*, 882−890.
40. Freimund, S., and Köpper, S. (2004) The composition of 2-keto aldoses in organic solvents as determined by NMR spectroscopy, *Carbohydr. Res. 339*, 217−220.
41. Köpper, S., and Freimund, S. (2003) The composition of keto aldoses in aqueous solution as determined by NMR spectroscopy, *Helv. Chim. Acta 86*, 827−843.
42. Baynes, J. W., and Thorpe, S. R. (1999) Role of oxidative stress in diabetic complications: a new perspective on an old paradigm, *Diabetes 48*, 1−9.
43. Chellan, P., and Nagaraj, R. H. (1999) Protein crosslinking by the Maillard reaction: dicarbonyl-derived imidazolium crosslinks in aging and diabetes, *Arch. Biochem. Biophys. 368*, 98−104.
44. Degenhardt, T. P., Thorpe, S. R., and Baynes, J. W. (1998) Chemical modification of proteins by methylglyoxal, *Cell. Mol. Biol. (Paris) 44*, 1139−1145.
45. Rosca, M. G., Mustata, T. G., Kinter, M. T., Ozdemir, A. M., Kern, T. S., Szweda, L. I., Brownlee, M., Monnier, V. M., and Weiss, M. F. (2005) Glycation of mitochondrial proteins from diabetic rat kidney is associated with excess superoxide formation, *Am. J. Physiol. Renal Physiol. 289*, F420−430.
46. Dobler, D., Ahmed, N., Song, L., Eboigbodin, K. E., and Thornalley, P. J. (2006) Increased dicarbonyl metabolism in endothelial cells in hyperglycemia induces anoikis and impairs angiogenesis by RGD and GFOGER motif modification, *Diabetes 55*, 1961−1969.
47. Chong, S. A., Lee, W., Arora, P. D., Laschinger, C., Young, E. W., Simmons, C. A., Manolson, M., Sodek, J., and McCulloch, C. A. (2007) Methylglyoxal inhibits the binding step of collagen phagocytosis, *J. Biol. Chem. 282*, 8510−8520.
48. Ahmed, N., and Thornalley, P. J. (2007) Advanced glycation endproducts: what is their relevance to diabetic complications, *Diabetes, Obes. Metab. 9*, 233−245.
49. Metzler, D. E., Ikawa, M., and Snell, E. E. (1954) A general mechanism for vitamin B6-catalyzed reactions, *J. Am. Chem. Soc. 76*, 648−652.
50. MacKenzie, K. E., Wiltshire, E. J., Gent, R., Hirte, C., Piotto, L., and Couper, J. J. (2006) Folate and vitamin B6 rapidly normalize endothelial dysfunction in children with type 1 diabetes mellitus, *Pediatrics 118*, 242−253.
51. Booth, A. A., Khalifah, R. G., and Hudson, B. G. (1996) Thiamine pyrophosphate and pyridoxamine inhibit the formation of antigenic advanced glycation end-products: comparison with aminoguanidine, *Biochem. Biophys. Res. Commun. 220*, 113−119.
52. Nakamura, S., and Niwa, T. (2005) Pyridoxal phosphate and hepatocyte growth factor prevent dialysate-induced peritoneal damage, *J. Am. Soc. Nephrol. 16*, 144−150.

BI701190S